Nanoparticle Electrical Analysis and Detection with a Solid-state Nanopore in a Microfluidic Device

Jean Roman, Olivier Français, Nathalie Jarroux, Gilles Patriarche, Juan Pelta, Bruno Le Pioufle, Laurent Bacri

Available online at www.sciencedirect.com

ScienceDirect

Procedia Engineering 168 (2016) 1475 – 1478

Procedia Engineering

www.elsevier.com/locate/procedia

30th Eurosensors Conference, EUROSENSORS 2016

Nanoparticle electrical analysis and detection with a solid-state nanopore in a microfluidic device

Jean Roman[a,b], Olivier Français[b], Nathalie Jarroux[a], Gilles Patriarche[c], Juan Pelta[a], Bruno Le Pioufle[b], Laurent Bacri[a,*]

[a] *Lambe UMR8587, University of Évry val d'Essonne, Évry 91000, France*
[b] *Satie UMR8029, ENS Cachan, Cachan 94230, France*
[c] *C2N UMR9001, Marcoussis 91460, France*

Abstract

Our society is increasingly exposed to harmful nano and nanobio particles as new viruses, harmful proteins (like prions) and metallic nanoparticles that need to be better detected and identified. Solid-state nanopores are rapidly growing candidates for fast and label-free electrical detection and analysis of nanoparticles. Being able to analyze each nanoparticle one at a time, the nanopore technology yields astonishing sensitivity results, a determining asset for early virus or pollutant detection. This proceeding describes our approach to develop an integrated sensor at the nanometer level.

Peer-review under responsibility of the organizing committee of the 30th Eurosensors Conference
Keywords: nanopores, single particle, DNA, translocation, protein, virus, electrical detection

1. Introduction

Inspired from biological channels[1], solid-state nanopores[2,3] appear to be one logical development of resistive pulse technologies[4–6]. These techniques rely on the use of a single nanopore pierced or inserted inside an insulating membrane. Applying a voltage bias across this membrane, we measure the ionic current going only through this pore. When a particle goes in the vicinity of the pore, the nanopore conductance decreases. This current drop reveals key features of the particle[7]. One major asset of solid-state nanopores is that their fabrication process allows the use of a wide span of sizes, from several nanometres to more than 100 nm, whereas only few sizes of biological channels are available (around 2nm). Nanoparticles just smaller than the pore will hardly be detected whereas the smallest ones won't block the pore enough to obtain a sufficient signal to noise ratio for proper data analysis. Using a solid-state nanopore we can fit our system to different nanoparticle sizes. Analysis of larger nanoparticles like viruses or metallic nanoparticles also becomes possible.

* Corresponding author. Tel.: +33-169-477-684.
E-mail address: laurent.bacri@univ-evry.fr

Peer-review under responsibility of the organizing committee of the 30th Eurosensors Conference
doi:10.1016/j.proeng.2016.11.425

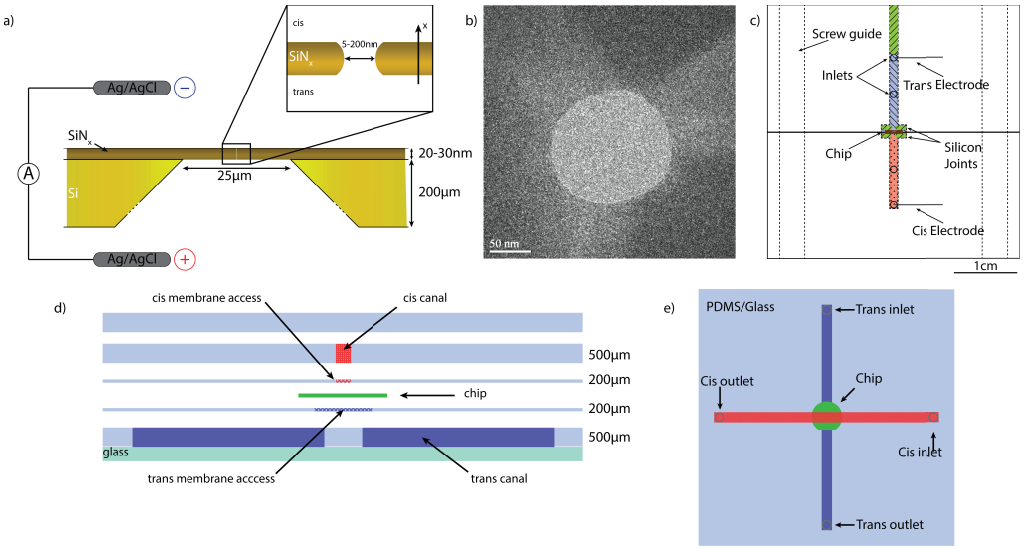

Fig. 1. (a) Schematic sectionnal view of a chip (not to scale). The SiN_x insulating membrane separates two electrolytes where Ag/AgCl electrodes; (b) TEM view of a TEM pierced 144nm pore in a 20nm thick SiN_x membrane. The same pore is used in the *Results and Discussion* section; (c) Schematic upper view of a classical fluidic setup around the nanopierced chip; (d) Exploded sectional view of the multi-layers microfluidic device (not to scale). Every slice but the silicon chip and the glass slide are made of PDMS; (e) Upper view of the microfluidic system, (not to scale).

We aim to develop an integrated system of solid-state nanopore analysis using microfluidics. Permitting a fast and reliable analysis of very small concentration and volume of nanoparticles directly on site would be an interesting add-on to the existing methods.

2. Material and Methods

The fabrication process of the chips we use follows three steps. 1) A 20nm thick SiN_x or SiO_2 low-stress layer is deposited over a 200μm thick silicon wafer using PECVD. 2) A 25x25μm window is etched in the silicon layer through Reactive Ion Etching (RIE). Multiple 3mm wide chips are obtained from one wafer and separated from each other thanks to the same RIE (Fig. 1.(a)). The thinner the membrane is, the better the resolution during the translocation of particles through the pore will be, but thinner membranes are also more fragile.The electric capacity formed by the membrane in contact with electrolytes tends to increase the noise of our electrical measurements[8]. To meet these expectations, our chips manufactured by Nanopore Solutions. 3) The nanopore is drilled by a custom TEM Jeol2200 as it permits high probe currents (up to 15nA): i) the electron beam of the TEM in scanning mode is focused on a small area of the membrane, ii) a nanopore is formed as the membrane heats up to sublimation. Real-time visualisation of the pore opening makes it possible to control precisely its size. Depending on the chosen probe current and the duration of exposure a pore up to 200nm is drilled (Fig. 1.(b)).

After optimising our macrofluidic set-up, a limit has been reached. To use even less particles we designed a microfluidic chip. A multi-layers PDMS (PolyDiMethylSiloxane) device has been devised (Fig. 1.(d)). PDMS has been chosen as a well-known biocompatible transparent material permitting optical measurement as well as electrical insulating and sealing around the silicon chip. The different layers of PDMS are covalently bonded to each other and to a supporting glass slide thanks to an O_2 plasma. The canals are performed using a photoresist resin mould (SU-8 2100). The thickness of 500μm we aim requires the resin to be spincoated twice. Insolation through a high resolution mask permits to obtain the needed geometry of the canals.

The *cis* reservoir is filled with a solution of 1 g/L 2 kbp salmon DNA (Sigma Aldrich), 0.1 M KCl and 25 mM Tris buffered at pH 8 whereas the *trans* reservoir contains a 0.1 M KCl, 25 mM Tris pH 8 buffered solution. Using Ag/AgCl electrodes we apply a voltage bias $U = 100\,mV$. The average value of the ionic current base across the membrane is $I_0 = 2050 \pm 11\,pA$. We calculate the pore conductance $G_{exp} = 20 \pm 1\,nS$ (Fig. 2.(a)).

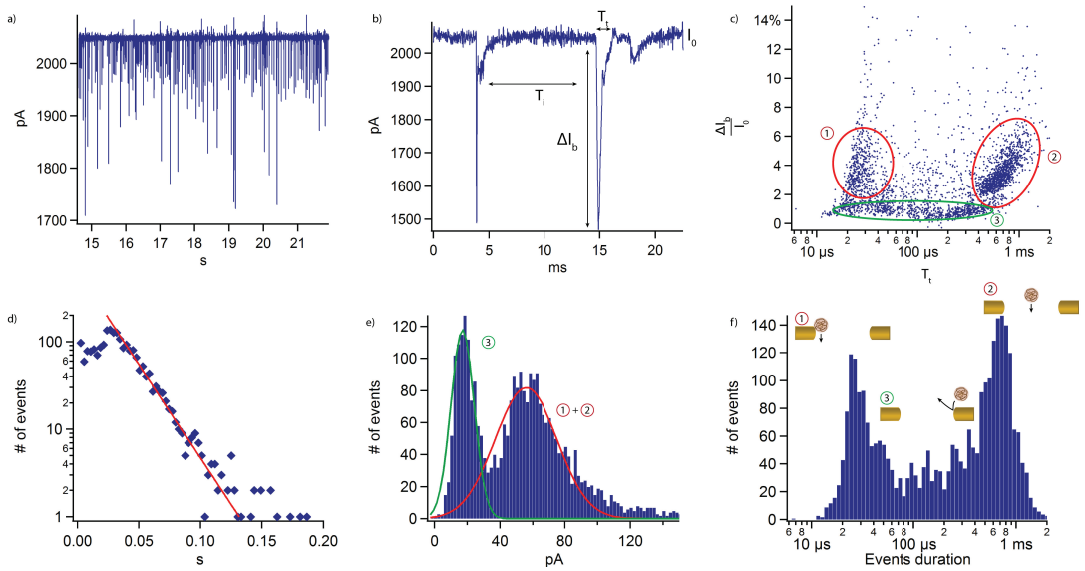

Fig. 2. (a) Illustration of the interesting parameters of current blockades: T_i the interevent time, T_t the event duration and I_b the current drop; (c) Current blockade normalized by average current versus event duration. Each point corresponds to a single event. Interaction types 1 and 2 are cycled in red and possibly correspond to translocation events whereas the third type correspong to bumping near and/or into the pore; (d) Histogram of the inter-event time fitted with an exponential fit to extract the critical frequency f_c of interaction; (e) Histogram of the blockade intensity ΔI_b featuring two gaussian distributions corresponding respectively to the assossiation of the first and second types of interaction and the third type; (f) Histogram of the events duration T_t and schematics of 1, 2 and 3 types interaction.

When a particle interacts with the pore, its ionic conductance transiently drops. Following a two thresholds method[9], each blockade is detected and characterized by 1) its amplitude ΔI_b, 2) its duration or dwelling time T_t 3) the duration between two following blockades or inter-event time T_i (Fig. 2.(b)). The detection of each current drop is performed by a home-made Igor Pro macro. The statistical analysis of all these blockades allows us to explore interactions between nanoparticles and the nanopore.

3. Results and discussion

This trace features a succession of blockades, characterized by their duration T_t, amplitude ΔI_b and inter-event time T_i Fig. 2.(b). The scatter plot shows three types of blockades Fig. 2.(c). The interpretation of Fig. 2.(d) leads to the characteristic blockade frequency $f_c = 32.9 \pm 1\,Hz$. In Fig. 2.(f) we observe interaction times corresponding to short $T_{t1} = 26 \pm 6\,\mu s$ and long $T_{t2} = 0.7 \pm 0.2\,ms$ blockades. The blockade amplitude distribution (Fig. 2.(e)) features two domains $\Delta I_{b1} = 17 \pm 7\,pA$ and $\Delta I_{b2} = 56 \pm 19\,pA$.

To discuss these observations, we first focus on the ionic nanopore conductance. In normal operating conditions, an open nanopore yields a conductance that only depends on its diameter $d = 145 \pm 6\,nm$, its length $\ell = 20\,nm$ and the conductivity $K = 1.2\,S/m$ of the buffer. Considering the resistivity $R_p = \dfrac{4\,\ell}{\pi K d^2}$ of a cylinder and access resistivity of a pore $R_a = \dfrac{1}{Kd}$ on a infinite flat surface, we evaluate the pore conductance $G_0 = \dfrac{1}{R_p + R_a}$. According to this formula we expect to have a conductance of $472 \pm 30\,nS$. This ionic conductance is 24 times higher than the measured one. DNA chains could stick to the inner part of the pore, decrease the apparent radius of the nanopore and modify the surface charge of nanopore. We use the relation above to determine the apparent pore diameter d_{app} from the conductance measurement. We solve $d_{app}^2 - \dfrac{G}{K}\,d_{app} - \dfrac{4}{\pi}\,\dfrac{G\,\ell}{K} = 0$ to obtain $d_{app} = 31 \pm 1$ nm. This diameter is almost five times lower than the expected value, showing that the inner wall of the nanopore is strongly covered by DNA strands.

Let us focus on the translocation process of DNA chains in the nanopore. At least two interaction types can be discriminated as we observe on Fig. 2.(c), (e). The first one, characterized by low blockades $\Delta I_{b1} = 17 \pm 7\,pA$, could be due to DNA bumping on the nanopore without translocating through it. These interactions are marked as type number 3 on Fig. 2.(c), (e) and (f). The second ones are deeper $\Delta I_{b2} = 56 \pm 19\,pA$ and could be due to the translocation process of the DNA coil (Fig. 2.(e)). The current blockade ratio is equal to $\rho = \Delta I_{b2}/I_0 = 2.7 \pm 0.7\,\%$. This ratio is given by the volume of the DNA V_{DNA} divided by the volume of the pore V_{pore}: $\rho = \dfrac{\frac{4}{3}\pi R_g^3}{\pi (d/2)^2\, \ell}$ where $R_g = N^{0.5} a/\sqrt{6} = 6.5\,\text{nm}$ is the giration radius of the DNA coil composed by N monomers of length $a = 0.35\,\text{nm}$. This relation allows us to determine the apparent pore nanopore diameter : $d_{app} = \sqrt{\dfrac{8}{3}\dfrac{R_g^3}{\rho\,\ell}} = 36 \pm 5\,\text{nm}$. This value is in good agreement with the one calculated from the pore conductance.

If we focus on dwell time T_t distribution, this transport is characterized by short and long dwell times, respectively (number 1 and 2 on Fig. 2.(c), (e) and (f)). The first ones are due to the transport of the chain directly through the nanopore, while the second one are due to strong interactions between chains and the inner part of the nanopore[10]. These dwell times have the same magnitude as previously observed with proteins[11], taking the difference of charge into account. As the blockade magnitude is the same in both regimes, the conformation of the DNA interacting or not with the pore is not dependent on the nature transport because the applied voltage is too low to uncoil the DNA[12].

4. Conclusion

From electrical measurements, we have shown that we can characterize the ionic flow through a nanopore and also the transport of DNA coils. The DNA coils could bump at the entrance of the nanopore, or enter inside it. During this transport process, two types of interactions between the analyte and the nanopore have been observed at the single molecule level : the DNA coil could stick the inner wall of the channel or directly goes through it. The DNA translocation is mainly controlled by interactions with the nanopore surface which must be reduced by chemical grafting. The integration of the nanopore device is under progress to reduce the already small amount of particles, the electrical noise and permit optical observation. This device shall go a step further toward on-field utilisation.

References

[1] J. J. Kasianowicz, E. Brandin, D. Branton, D. W. Deamer, Characterization of individual polynucleotide molecules using a membrane channel., Proc Natl Acad Sci USA 93 (1996) 13770–13773.
[2] J. Li, D. Stein, C. McMullan, D. Branton, M. J. Aziz, J. A. Golovchenko, Ion-beam sculpting at nanometre length scales., Nature 412 (2001) 166–169.
[3] S. W. Kowalczyk, L. Kapinos, T. R. Blosser, T. Magalhes, P. van Nies, R. Y. H. Lim, C. Dekker, Single-molecule transport across an individual biomimetic nuclear pore complex., Nat Nanotechnol 6 (2011) 433–438.
[4] M. Wanunu, W. Morrison, Y. Rabin, A. Y. Grosberg, A. Meller, Electrostatic focusing of unlabelled dna into nanoscale pores using a salt gradient., Nat Nanotechnol (2010).
[5] C. Plesa, J. W. Ruitenberg, M. J. Witteveen, C. Dekker, Detection of individual proteins bound along dna using solid-state nanopores, Nano Lett. 15 (2015) 3153–3158.
[6] D. Branton, D. W. Deamer, A. Marziali, H. Bayley, S. A. Benner, T. Butler, M. D. Ventra, S. Garaj, A. Hibbs, X. Huang, S. B. Jovanovich, P. S. Krstic, S. Lindsay, X. S. Ling, C. H. Mastrangelo, A. Meller, J. S. Oliver, Y. V. Pershin, J. M. Ramsey, R. Riehn, G. V. Soni, V. Tabard-Cossa, M. Wanunu, M. Wiggin, J. A. Schloss, The potential and challenges of nanopore sequencing., Nat Biotechnol 26 (2008) 1146–1153.
[7] L. Bacri, A. G. Oukhaled, B. Schiedt, G. Patriarche, E. Bourhis, J. Gierak, J. Pelta, L. Auvray, Dynamics of colloids in single solid-state nanopores., J Phys Chem B 115 (2011) 2890–2898.
[8] A. Balan, B. Machielse, D. Niedzwiecki, J. Lin, P. Ong, R. Engelke, K. L. Shepard, M. Drndić, Improving signal-to-noise performance for dna translocation in solid-state nanopores at mhz bandwidths (2014).
[9] A. Oukhaled, L. Bacri, M. Pastoriza-Gallego, J.-M. Betton, J. Pelta, Sensing proteins through nanopores: Fundamental to applications., ACS Chem Biol (2012).
[10] D. Pedone, M. Firnkes, U. Rant, Data analysis of translocation events in nanopore experiments., Anal Chem 81 (2009) 9689–9694.
[11] A. Oukhaled, B. Cressiot, L. Bacri, M. Pastoriza-Gallego, J.-M. Betton, E. Bourhis, R. Jede, J. Gierak, L. Auvray, J. Pelta, Dynamics of completely unfolded and native proteins through solid-state nanopores as a function of electric driving force, ACS Nano (2011).
[12] B. Cressiot, A. Oukhaled, G. Patriarche, M. Pastoriza-Gallego, J.-M. Betton, L. Auvray, M. Muthukumar, L. Bacri, J. Pelta, Protein transport through a narrow solid-state nanopore at high voltage: Experiments and theory., ACS Nano (2012).